Journal of the Serbian Society for Computational Mechanics / Vol. 15 / No. 2, 2021 / pp 79-92
(10.24874/jsscm.2021.15.02.08)

BLOOD FLOW IN ARTERIAL BIFURCATION CALCULATED BY TURBULENT FINITE ELEMENT MODEL

Aleksandar Nikolić[1*], Marko Topalović[1], Vladimir Simić[1], Milan Blagojević[2]

[1] Department of Technical-Technological Sciences, Institute for Information Technologies, University of Kragujevac, Kragujevac, Serbia
e-mail: dziga@kg.ac.rs, topalovic@kg.ac.rs, vsimic@kg.ac.rs
[2] Faculty of Technical Sciences, University of Priština, Kosovska Mitrovica, Serbia
e-mail: milan.blagojevic@pr.ac.rs
**corresponding author*

Abstract

In this paper, numerical analysis of turbulent fluid flow is presented. Finite Element Method is used combining implicit integration with Eulerian spatial formulation, i.e. nodes and geometry are fixed in time. Characteristic values, such as fluid pressure and velocity, kinetic energy, turbulence, and dissipation of turbulent kinetic energy, are calculated in the finite element nodes for each step of the incremental-iterative procedure. For calculation of characteristic values, a two-equation model in the viscous sublayer is implemented. The main goal of our research was development of flexible methodology for application of proposed numerical procedures in the clinical studies. It was achieved in three steps: first was implementation of the turbulent finite element model in in-house solver PAK, the second step was development of the software for customized generation of finite element meshes for biological shapes, and the final step (which was the main focus of this paper) was the analysis of complex blood flow problems inside the bifurcation of arteries. Results shows that the proposed tools and methods can be used by cardiologist or vascular surgeons for investigating the hemodynamic conditions inside patient specific blood vessels. This would allow them better customization of drug treatment and planning of operation if one is needed.

Keywords: Fluid flow, turbulent flow, finite element, simulation, $k-\omega$ model

1. Introduction

Blood flow through the cardiovascular system is one of the most important and studied phenomena in bioengineering Kojić et al. (2008). Fluid flow in general can be laminar or turbulent. is. In laminar flow fluid layers move in parallel, hence it is more energy-efficient. while in the turbulent flow we have swirling vortexes and eddies. Turbulent flow occurs in the narrowing of the blood vessels, when the flow velocity exceeds a certain value, or when the blood suddenly slows down due to the obstacles like stenosis. Laminar flow is the default blood behavior, but for the doctors dealing with cardio-vascular conditions, turbulent flow is more interesting. In order to predict further development of disease, they need velocity and pressure fields, wall sheer stress and oscillatory shear index which can be used to predict plaque formation.

Blood is the most important fluid in the human body that carry oxygen, nutrients, , hormones and other crucial chemicals. Although all these inclusions have different properties, due to their relative size in comparison to the analyzed geometry of the vessel, blood is modelled as a homogenous fluid with averaged viscosity properties, according to Shi et al. (2011). Transport of the moleculs is governed by convective-diffusive laws. With blood approximated as a incompressible homogenous viscous fluid, the flow in blood vessels can be modelled by the Navier–Stokes equations and incompressibility equation (Kojić et al. 2017).

Plaque deposition in the cardiovascular system that causes atherosclerosis occurs primarily in the branches, where the arteries have a complex geometry (Soulis et al. 2011). This complex geometry governs the flow, which is according to (Weydahl et al. 2001) specific for each patient Yet, so far, most of the flow calculations were done on the averaged or idealized geometries. This causes significant deviations from the solutions obtained by patient specific modeling of the blood vessel (Owida et al. 2012). The advances in the fields of radiological diagnostics and increased computer performance, were necessary conditions for patient specific treatment, as can be seen in (Owida et al. 2012) and (Goubergrits et al. 2003). But, this raw data is useless unless we have comprehensive software solutions for its processing and analysis, which was the main scientific contribution of our work, and will be the future focus of our research with continuous improvements and development.

The statistical modeling of turbulence requires approximation of the fluid velocity as the sum of the average values of velocity and velocity fluctuations around that value (McDonough 2007). Reynolds equations are obtained from the Navier-Stokes equations using this approximations according to (Wilcox 1988). The new components in these equations are called turbulent or Reynolds stresses. Model $k-\omega$ has been introduced by (Wilcox 1994) and (Wilcox 2006) to predict turbulent flow. This model is unjustly neglected in biomechanical and medical research, the fact on which we must shed light on in our numerical simulations.

In-house Finite Element Method (FEM) solver PAK that we use in our research is based on theory developed and summarized by Bathe (2006). Reynolds equations and $k-\omega$ turbulent model coupling is done according to (Bassi et al. 2005) and (Bassi et al. 2014). For the verification and comparison with the experimental results published by (Jovic et al. 1994) we used example of a channel with a backward-facing step. Analysis with the FEM $k-\omega$ model corresponds well with the experimental results published by (Jovic et al. 1994) The innovative implementation of the $k-\omega$ model in bioengineering, presented in this paper will enable doctors analyze the development of cardiovascular problems for specific patients and to decide the most appropriate treatmentor surgery. Using PAK software doctors can observe how stenosis can cause the transition from laminar to turbulent flow, Also the can see that changes of shears stress on the blood vessel wall can increase the risk of plaque formation.

Carotid artery geometries used in our research, were obtained from radiological scans of several anonymous patients. The methodology of generating a quality finite element mesh using STL2FEM software is described in detail in Blagojević et al. (2013). This software uses volumetric model obtained by radiological imaging to generate a block topology, which is afterwards used for generating finite elements using the multi-block method (Blagojević et al. 2013) and (Arbogast et al. 2000). For the particular patient whose carotid artery is best suited to show the capabilities of the developed software, fluid velocity, pressure field and shear stress is shown.

2. Methods

2.1 Basic equations of turbulent flow and k-ω model

All computational turbulent models are based on Reynolds equations and Boussinesq approximation (Boussinesq 1877), (McDonough 2007). Each model has form of one-equation or two-equations that explains turbulent quantities. Boussinesq approximation is used for members of the Reynolds equations where turbulent stresses are approximated by turbulent dynamic viscosity.

$k-\omega$ turbulent model is commonly used for modeling the turbulent problems. It was presented for the first time in the papers of Wilcox (Wilcox 1988, Wilcox 1994 and Wilcox 2006). Since then, this model has not been significantly modified.

$k-\omega$ turbulent model has two equations, equation for kinetic energy of turbulence and equation for specific dissipation of the kinetic energy of turbulence. Model don't need wall functions for calculating fluid flow near the walls of problem following Wilcox (1988) and Ferziger et al. (2002).

Later, turbulent model $k-\omega$ was improved to version with low Reynolds number. Discontinuous Galerkin method is implemented for numerical algorithms for discretization following papers of Li et al. (2018) and Tomboulides et al. (2018).

The Reynolds Averaged Navier-Stokes (RANS) are based on the Navier-Stokes equation and the equation of continuity and represent the first part in modeling of turbulence by statistical methods:

$$\rho\left[\frac{\partial\overline{v}_i}{\partial t}+\overline{v}_j\frac{\partial\overline{v}_i}{\partial x_j}\right]=-\frac{\partial\overline{p}}{\partial x_i}+\frac{\partial}{\partial x_j}\left[\left(\mu_{eff}\right)\left(\frac{\partial\overline{v}_i}{\partial x_j}+\frac{\partial\overline{v}_j}{\partial x_i}\right)\right], \tag{1}$$

$$\frac{\partial\overline{v}_i}{\partial x_i}=0\,, \tag{2}$$

where μ_{eff} is the effective dynamic viscosity defined by the sum of dynamic viscosity and turbulent dynamic viscosity:

$$\mu_{eff}=\mu+\mu_T\,. \tag{3}$$

In $k-\omega$ turbulent model, turbulent dynamic viscosity of fluid μ_T is calculated by turbulent kinetic energy and specific dissipation of the kinetic energy of turbulence as:

$$\mu_T=\alpha^*\frac{k}{\omega}\,. \tag{4}$$

Equation for the kinetic energy of the turbulence k is defined following McDonough (2007) as:

$$\rho\left(\frac{\partial k}{\partial t}+\overline{v}_j\frac{\partial k}{\partial x_j}\right)=\frac{\partial}{\partial x_j}\left[\left(\mu+\sigma^*\mu_T\right)\frac{\partial k}{\partial x_j}\right]+P_k-\beta_k\rho k\omega\,, \tag{5}$$

where P_k represents the effect of kinetic energy of turbulence and is defined as:

$$P_k = \mu_T \left(\frac{\partial \overline{v_i}}{\partial x_j} + \frac{\partial \overline{v_j}}{\partial x_i} \right) \frac{\partial \overline{v_i}}{\partial x_j} \tag{6}$$

Second variable, specific dissipation of the kinetic energy of turbulence ω is defining the scale of turbulence and can be calculated by next equation:

$$\rho \left(\frac{\partial \omega}{\partial t} + \overline{v}_j \frac{\partial \omega}{\partial x_j} \right) = \frac{\partial}{\partial x_j} \left[\left(\mu + \sigma \mu_T \right) \frac{\partial \omega}{\partial x_j} \right] + \alpha_k \frac{\omega}{k} P_k - \beta_\omega \rho \omega^2 \tag{7}$$

In equations (5) и (7) constants α^*, α, β_ω, β_k, σ and σ^* have the following values according to Wilcox (1988) and Wilcox (2006):

$$\alpha^* = 1, \quad \alpha_k = \frac{5}{9}, \quad \beta_\omega = \frac{3}{40}, \quad \beta_k = \frac{9}{100}, \quad \sigma = \frac{1}{2}, \quad \sigma^* = \frac{1}{2} \tag{8}$$

2.2 Finite element formulation of RANS equations and k-ω model

In the previous section, we show basic equations that are solved for turbulent fluid flow are the RANS equations represented by the equations (1) and (2). For each finite element, velocity of fluid $\mathbf{v}(x,y,z)$ is approximated by a velocity vector $\mathbf{v}(r,s,t)$ where r, s, t are the local coordinates of the finite element according to Kojić et al. (2008) and Bathe (2006). Fluid velocity in each finite element node can be written by the velocity vector $\mathbf{v}$ as:

$$v_i = \sum_{I=1}^{N} h_I V_i^I \equiv h_I V_i^I, \qquad \mathbf{v} = \mathbf{H}\mathbf{V}, \qquad i = 1, 2, 3; \quad I = 1, 2, ..., N \tag{9}$$

where h_k are the interpolation functions, V_i^I are the components (x, y, z) of the fluid velocity vector for the node I and N represent total number of the finite element nodes. The governing equations (5) and (7) for $k-\omega$ model can be converted to the finite element equations of balance for a single finite element by implementing a standard Galerkin weighting method (Milosevic et al. 2018). Applying a Galerkin method to equations (1), (2), (5) and (7) using the interpolation functions for fluid velocity, the pressure, kinetic energy k and specific dissipation ω given with (Kojić et al. 2008 and Bathe 2006):

$$\overline{v}_i = h_\mathrm{I} \overline{V_i^\mathrm{I}} \tag{10}$$

$$\overline{p}_i = \hat{h}_\mathrm{I} P_\mathrm{I} \tag{11}$$

$$k = h_\mathrm{I} k^\mathrm{I} \tag{12}$$

$$\omega = h_\mathrm{I} \omega^\mathrm{I} \tag{13}$$

The previous equations are obtained in the matrix form:

$$\begin{bmatrix} \mathbf{M} & 0 \\ 0 & 0 \end{bmatrix} \begin{bmatrix} \dot{\mathbf{V}} \\ \dot{\mathbf{P}} \end{bmatrix} + \begin{bmatrix} \mathbf{K}_{\mathrm{vv}} + \mathbf{K}_{\mu \mathrm{vt}} & \mathbf{K}_{\mathrm{vp}} \\ \mathbf{K}_{\mathrm{vp}}{}^{\mathrm{T}} & 0 \end{bmatrix} \begin{bmatrix} \mathbf{V} \\ \mathbf{P} \end{bmatrix} = \begin{bmatrix} \mathbf{F}_\mathrm{v} + \mathbf{F}_\mathrm{s} \\ 0 \end{bmatrix} \tag{14}$$

The components of these submatrices and subvectors are:

$$\left(\bar{\mathbf{M}}\right)_{\mathrm{IJ}} = \rho \int_V h_{\mathrm{I}} h_{\mathrm{J}} dV \tag{15}$$

$$\left(\bar{\mathbf{K}}_{\mathrm{vv}}\right)_{\mathrm{IJ}} = \rho \int_V h_{\mathrm{I}} h_{\mathrm{K}} \overline{V_j}^{\mathrm{I}} h_{\mathrm{J},j} dV \tag{16}$$

$$\left(\bar{\mathbf{K}}_{\mu\mathrm{vt}}\right)_{\mathrm{IJ}} = \int_V \left(\mu + \mu_T\right) h_{\mathrm{I},j} h_{\mathrm{J},j} dV \tag{17}$$

$$\left(\mathbf{K}_{\mathrm{vpi}}\right)_{\mathrm{IJ}} = -\int_V h_{\mathrm{I},i} \widehat{h}_{\mathrm{J}} dV \tag{18}$$

$$\left(\mathbf{F}_{\mathrm{vi}}\right)_{\mathrm{I}} = \rho \int_V h_{\mathrm{I}} f_i^V dV \tag{19}$$

$$\left(\mathbf{F}_{\mathrm{si}}\right)_{\mathrm{I}} = \int_S h_{\mathrm{I}} \left[-\bar{p} n_i + \left(\mu + \mu_T\right) \overline{V_{i,j}}^{\mathrm{I}} n_j \right] dS \tag{20}$$

For the turbulent model $k-\omega$, finite element equations are derived from equations (5) and (7) formulated as:

$$\left[\mathbf{M_K}\right]\left[\dot{\mathbf{k}}\right] + \left[\mathbf{K_{VK}} + \mathbf{K_{MK}} + \mathbf{K_{\beta k}}\right]\left[\mathbf{k}\right] - \left[\mathbf{K_{VV1}}\right]\left[\mathbf{V}\right] = \mathbf{F_{SK2}} \tag{21}$$

$$\left[\mathbf{M_K}\right]\left[\dot{\boldsymbol{\omega}}\right] + \left[\mathbf{K_{VK}} + \mathbf{K_{M\omega}} + \mathbf{K_{\beta\omega}}\right]\left[\boldsymbol{\omega}\right] - \left[\mathbf{K_{VV2}}\right]\left[\mathbf{V}\right] = \mathbf{F_{S\omega}} \tag{22}$$

The components of submatrices and subvectors for the equation (21) are:

$$\left(\mathbf{M_K}\right)_{\mathrm{IJ}} = \rho \int_V h_{\mathrm{I}} h_{\mathrm{J}} dV \tag{23}$$

$$\left(\mathbf{K_{VK}}\right)_{\mathrm{IJ}} = \rho \int_V h_{\mathrm{I}} h_{\mathrm{J}} \overline{V_i^{\mathrm{J}}} h_{\mathrm{I},j} dV \tag{24}$$

$$\left(\mathbf{K_{MK}}\right)_{\mathrm{IJ}} = \int_V \left(\mu + \sigma^* \mu_T\right) h_{\mathrm{I},j} h_{\mathrm{J},j} dV \tag{25}$$

$$\left(\mathbf{K_{\beta k}}\right)_{\mathrm{IJ}} = \rho \beta_k \theta \int_V h_{\mathrm{I}} h_{\mathrm{J}} h_{\mathrm{K}} k^{\mathrm{J}} dV \tag{26}$$

$$\left(\mathbf{K_{VV1}}\right)_{\mathrm{IJ}} = 2 \int_V \mu_T h_{\mathrm{I}} h_{\mathrm{J},j} \overline{V_i^{\mathrm{J}}} h_{\mathrm{K},j} dV \tag{27}$$

$$\left(\mathbf{F_{SK2}}\right)_{\mathrm{I}} = \left(\mu + \sigma^* \mu_T\right) \int_S h_{\mathrm{I}} k_{,j} n_j dS \tag{28}$$

The components of submatrices and subvectors are for the equation (22):

$$\left(\mathbf{K_{M\omega}}\right)_{\mathrm{IJ}} = \left[\int_V \left(\mu + \sigma \mu_T\right) h_{\mathrm{I},j} h_{\mathrm{J},j} dV \right] \tag{29}$$

$$\left(\mathbf{K}_{\boldsymbol{\beta\omega}}\right)_{\mathrm{IJ}} = \rho\beta_{\omega}\int_{V} h_{\mathrm{I}}h_{\mathrm{J}}h_{\mathrm{K}}\omega^{\mathrm{J}}dV \tag{30}$$

$$\left(\mathbf{K}_{\mathbf{VV2}}\right)_{\mathrm{IJ}} = 2\alpha_k\theta\mu_T\int_{V} h_{\mathrm{I}}h_{\mathrm{J},j}\overline{V_i^{\mathrm{J}}}h_{\mathrm{K},j}dV \tag{31}$$

$$\left(\mathbf{F}_{\mathbf{S\omega}}\right)_{\mathrm{I}} = \left(\mu+\sigma\mu_T\right)\int_{S} h_{\mathrm{I}}\omega_{,j}n_j dS \tag{32}$$

If Reynolds equations (14) are coupled with equations (21) and (22) we have the following system of equations in matrix form:

$$\begin{bmatrix} \mathbf{M}_{\mathbf{V}} & 0 & 0 & 0 \\ 0 & 0 & 0 & 0 \\ 0 & 0 & \mathbf{M}_{\mathbf{K}} & 0 \\ 0 & 0 & 0 & \mathbf{M}_{\mathbf{K}} \end{bmatrix}\begin{bmatrix} \dot{\mathbf{V}} \\ \dot{\mathbf{P}} \\ \dot{\mathbf{k}} \\ \dot{\boldsymbol{\omega}} \end{bmatrix} + \begin{bmatrix} \mathbf{K}_{\mathrm{vv}}+\mathbf{K}_{\mu\mathrm{vt}} & \mathbf{K}_{\mathrm{vp}} & 0 & 0 \\ \mathbf{K}_{\mathrm{vp}}^{\mathrm{T}} & 0 & 0 & 0 \\ -\mathbf{K}_{\mathbf{VV1}} & 0 & \mathbf{K}_{\mathbf{VK}}+\mathbf{K}_{\mathbf{MK}}+\mathbf{K}_{\boldsymbol{\beta k}} & 0 \\ -\mathbf{K}_{\mathbf{VV2}} & 0 & 0 & \mathbf{K}_{\mathbf{VK}}+\mathbf{K}_{\mathbf{M\omega}}+\mathbf{K}_{\boldsymbol{\beta\omega}} \end{bmatrix}\begin{bmatrix} \mathbf{V} \\ \mathbf{P} \\ \mathbf{k} \\ \boldsymbol{\omega} \end{bmatrix} = \begin{bmatrix} \mathbf{F}_{\mathrm{v}}+\mathbf{F}_{\mathrm{s}} \\ 0 \\ \mathbf{F}_{\mathbf{SK2}} \\ \mathbf{F}_{\mathbf{S\omega}} \end{bmatrix} \tag{33}$$

2.3 Incremental-iterative procedure for solving nonlinear equations

The fluid velocity in the convection member in equation (33) make this equation nonlinear, so incremental-iterative procedure is used for solving following Kojić et al. (2008).

The fluid velocity, the pressure, kinetic energy k and specific dissipation ω at the end of the time step ($t+\Delta t$) can be calculated as the values from the previous iteration ($i-1$) and the increment from current iteration (i) following Nikolić et al. (2021):

$${}^{t+\Delta t}\overline{V_i^{\mathrm{I}}} = {}^{t+\Delta t}\overline{V_i^{\mathrm{I}}}^{(i-1)} + \Delta\overline{V_i^{\mathrm{I}}}^{(i)} \tag{34}$$

$${}^{t+\Delta t}P_{\mathrm{I}} = {}^{t+\Delta t}P_{\mathrm{I}}^{(i-1)} + \Delta P_{\mathrm{I}}^{(i)} \tag{35}$$

$${}^{t+\Delta t}k^{\mathrm{I}} = {}^{t+\Delta t}k^{\mathrm{I}(i-1)} + \Delta k^{\mathrm{I}(i)} \tag{36}$$

$${}^{t+\Delta t}\omega^{\mathrm{I}} = {}^{t+\Delta t}\omega^{\mathrm{I}(i-1)} + \Delta\omega^{\mathrm{I}(i)} \tag{37}$$

where i is the current iteration number. Then, variables from eqs. (34) to (37) can be derived by the time via Euler's forward scheme:

$${}^{t+\Delta t}\dot{\overline{V_i^{\mathrm{I}}}} = \frac{{}^{t+\Delta t}\overline{V_i^{\mathrm{I}}} - {}^{t}\overline{V_i^{\mathrm{I}}}}{\Delta t} = \frac{{}^{t+\Delta t}\overline{V_i^{\mathrm{I}}}^{(i-1)} + \Delta\overline{V_i^{\mathrm{I}}}^{(i)} - {}^{t}\overline{V_i^{\mathrm{I}}}}{\Delta t} \tag{38}$$

$${}^{t+\Delta t}\dot{k}^{\mathrm{I}} = \frac{{}^{t+\Delta t}k^{\mathrm{I}} - {}^{t}k^{\mathrm{I}}}{\Delta t} = \frac{{}^{t+\Delta t}k^{\mathrm{I}(i-1)} + \Delta k^{\mathrm{I}(i)} - {}^{t}k^{\mathrm{I}}}{\Delta t} \tag{39}$$

$${}^{t+\Delta t}\dot{\omega}^{\mathrm{I}} = \frac{{}^{t+\Delta t}\omega^{\mathrm{I}} - {}^{t}\omega^{\mathrm{I}}}{\Delta t} = \frac{{}^{t+\Delta t}\omega^{\mathrm{I}(i-1)} + \Delta\omega^{\mathrm{I}(i)} - {}^{t}\omega^{\mathrm{I}}}{\Delta t} \tag{40}$$

If we use equations (34), (35) and (38) in the equation (14) we get the iterative-incremental equation:

$$\begin{bmatrix} \frac{1}{\Delta t}\mathbf{M} + {}^{t+\Delta t}\mathbf{K}_{vv}{}^{(i-1)} + {}^{t+\Delta t}\mathbf{K}_{\mu vt}{}^{(i-1)} + {}^{t+\Delta t}\mathbf{J}_{vv}{}^{(i-1)} & \mathbf{K}_{vp} \\ \mathbf{K}_{vp}{}^{T} & 0 \end{bmatrix} \begin{Bmatrix} \Delta\mathbf{V}^{(i)} \\ \Delta\mathbf{P}^{(i)} \end{Bmatrix} = \begin{Bmatrix} {}^{t+\Delta t}\mathbf{F}_{\mathbf{B}}{}^{(i-1)} \\ {}^{t+\Delta t}\mathbf{F}_{\mathbf{P}}{}^{(i-1)} \end{Bmatrix} \tag{41}$$

If equations (34), (36) and (37) are combined with equations (38), (39) and (40) we get the next equation:

$$\begin{bmatrix} {}^{t+\Delta t}\mathbf{K}_{\mathbf{KV}}{}^{(i-1)} + {}^{t+\Delta t}\mathbf{K}_{\mathbf{VVK}}{}^{(i-1)} & 0 & 0 \\ 0 & \frac{1}{\Delta t}\mathbf{M} + {}^{t+\Delta t}\mathbf{K}_{\mathbf{VK}}{}^{(i-1)} + {}^{t+\Delta t}\mathbf{K}_{\mathbf{MK}}{}^{(i-1)} + {}^{t+\Delta t}\mathbf{K}_{\beta\mathbf{k}}{}^{(i-1)} & 0 \\ {}^{t+\Delta t}\mathbf{K}_{\omega\mathbf{V}}{}^{(i-1)} + {}^{t+\Delta t}\mathbf{K}_{\mathbf{VV}\omega}{}^{(i-1)} & 0 & \frac{1}{\Delta t}\mathbf{M} + {}^{t+\Delta t}\mathbf{K}_{\mathbf{VK}}{}^{(i-1)} + {}^{t+\Delta t}\mathbf{K}_{\mathbf{M}\omega}{}^{(i-1)} + {}^{t+\Delta t}\mathbf{K}_{\beta\omega}{}^{(i-1)} \end{bmatrix} \begin{Bmatrix} \Delta\mathbf{V}^{(i)} \\ \Delta\mathbf{k}^{(i)} \\ \Delta\boldsymbol{\omega}^{(i)} \end{Bmatrix} = \begin{Bmatrix} {}^{t+\Delta t}\mathbf{R}_{\mathbf{V}}{}^{(i-1)} \\ {}^{t+\Delta t}\mathbf{R}_{\mathbf{K}}{}^{(i-1)} \\ {}^{t+\Delta t}\mathbf{R}_{\omega}{}^{(i-1)} \end{Bmatrix} \tag{42}$$

An algorithmic scheme is defined to explain the coupling of RANS equations and turbulent model $k-\omega$ as:

1. Calculating initialization parameters for turbulent flow (dynamic turbulent viscosity at the start of problem μ_{T0}, kinetic energy of the turbulence at the start of problem k_0, specific dissipation of the kinetic energy of turbulence at the start of problem ω_0, turbulent length l_T).

2. Starting loop with solving of equation (41) using dynamic turbulent viscosity from previous step ${}^{t+\Delta t}\mu_T{}^{(i-1)}$.

3. Solving equations (21) and (22) using fluid velocity ${}^{t+\Delta t}\overline{V_i^{\mathrm{I}}}^{(i-1)}$ from the previous step and calculating dynamic turbulent viscosity in the current step ${}^{t+\Delta t}\mu_T{}^{(i)}$.

4. End of loop.

In this scheme steps 2 and 3 are repeated until calculation come to the final step. Results of simulation is the saved in commonly used outputs such as a post-processing software ParaView (James et al. 2005).

3. Simulation of blood flow in arterial bifurcation

The original CT images in DICOM format that contain data on the tissues of the carotid arteries, were imported by MIMICS software (B. Materialise NV 2017). On the Fig. 1. (a) model of carotid artery bifurcation in STL file format is presented while on the Fig. 1. (b) we presented blocks of finite elements created by STL2FEM in-house software (Blagojević et al. 2013) and (Blagojević et al. 2014).

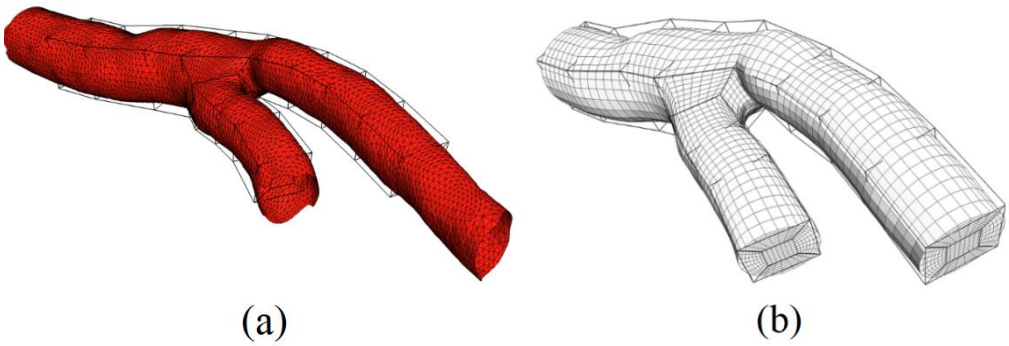

Fig. 1. (a) Model of carotid artery bifurcation in STL file format, (b) Blocks of finite elements created by STL2FEM.

Blood flow through the blood vessel was simulated on the real finite element model of the carotid artery of the selected patient (Blagojević et al. 2013 and Conti et al. 2016). PAK software was used for the calculation of blood flow (Kojić et al. 2020). The calculation was created in 200-time steps with an interval of 0.005s. Turbulent finite element model developed by Nikolić et al. (2021) is used. The finite element model has 67908 3D hexahedral elements which is showed on Fig. 2.

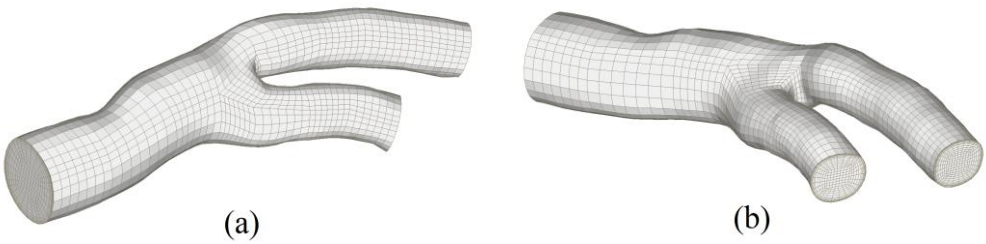

Fig. 2. Carotid artery bifurcation finite element model, a) from the front, b) from the back.

One cardiac cycle (systole and diastole) is used as time function in the calculation, Fig. 3, (Blagojević et al. 2014). Steps that are important for bioengineering analysis are rounded on Fig. 3, peak of systole (step 21), end of systole (step 42) and long period of diastole (step 160).

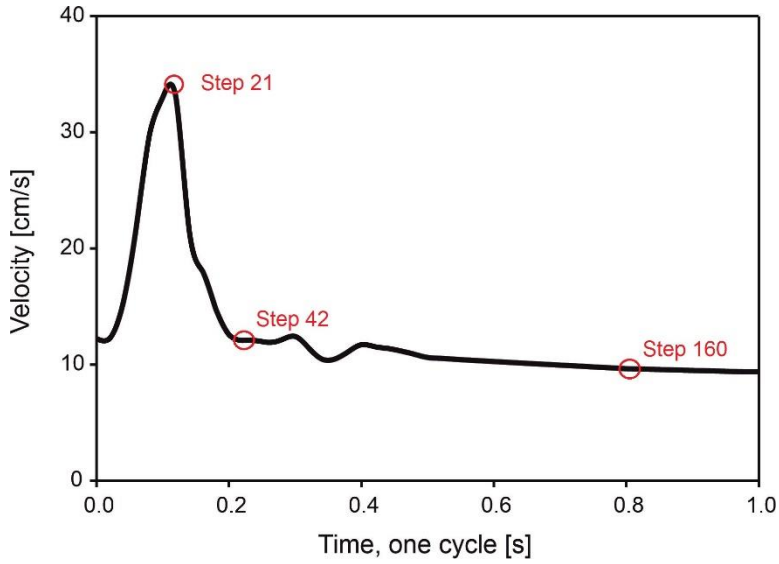

Fig. 3. The cardiac cycle that is used as inlet time function for the velocity of blood.

The boundary conditions that are applied to the problem are:

a) at the input we set parabolic velocity profile,

b) on the surfaces on the output branches of the model there is resistance that occurs because the blood flow continues through other blood organs. It is a condition that surface forces at the outlet are zero. It is can be explained by the equation (Nikolić et al. (2021)):

$$-p_i + \frac{1}{R_e}\frac{\partial \overline{v}_i}{\partial x_j} n_j = 0 \tag{43}$$

If the pressure is not prescribed on the outlet cross-section, as a boundary condition, the result is a pressure drop field in the modeled domain. Blood is considered as Newton's viscous fluid with material characteristics as: density of fluid $\rho = 1050 kg/m^3$ and dynamic viscosity of fluid $\mu = 3.675 * 10^{-3} kg/ms$. From references and experimental papers, it was conducted that the average value of blood velocity is $v_T = 33 cm/s$ for carotid artery.

The Reynolds number in this problem calculated for inlet diameter of $d = 0.72 cm$ is $\mathrm{Re} = 679$. Blood flow velocity results are represented by sections through the carotid artery and showed on Fig. 4. Results are divided in three sections for important steps in analysis, pick of systole (step 21), end of systole (step 42) and stationary period of diastole (step 160).

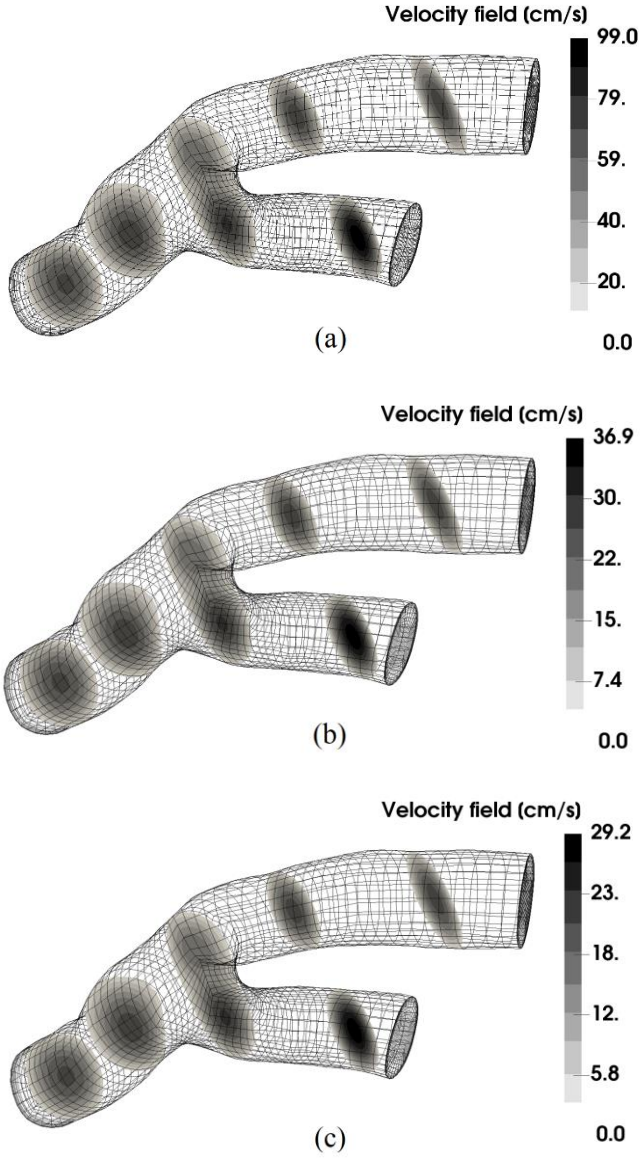

Fig. 4. Section cuts of velocity field, (a) step 21, (b) step 42, (c) step 160.

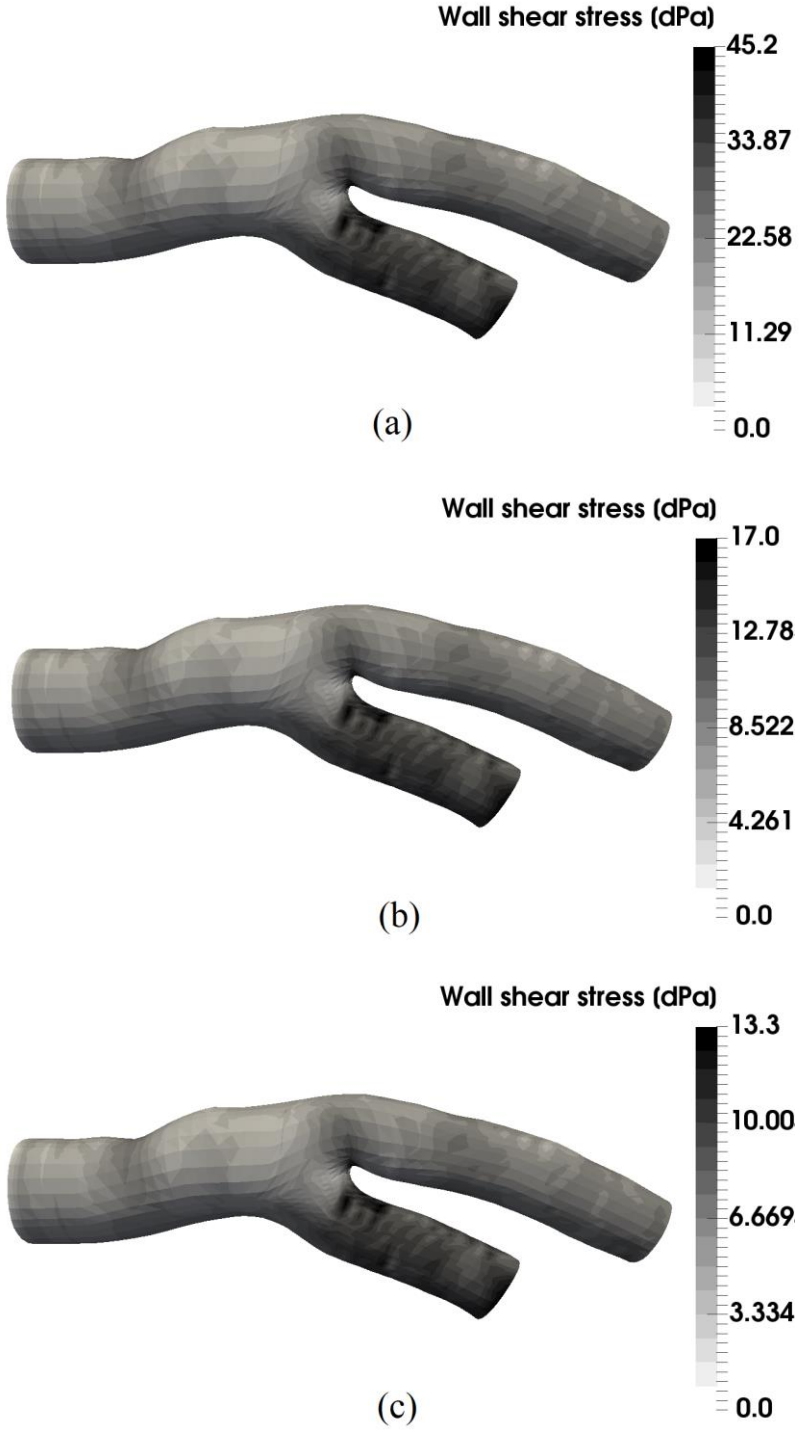

Fig. 5. Wall shear stress on carotid artery bifurcation, (a) step 21, (b) step 42, (c) step 160.

The wall shear stress results are shown in Fig. 5 for the most important steps of analysis: step 21, step 42 and step 160.

In addition, one more comparison is added. In Fig. 6, the laminar and turbulent velocity case is presented. On the left column, results for laminar flow is shown for Reynolds number 679. Right column are results for a turbulent case and Reynolds number 679. Regarding the presented results, it is notable that solutions given for turbulent yields flow, compared to results obtained for the field of laminar flow, differ in an acceptable range. Disagreement is mostly present in observing the shear stress values in the artery wall. Usage of quantification methods like oscillatory shear index (OSI) and wall shear stress (WSS) had a significant impact on the interpretation of the turbulent field of results, typically in those areas where increase of fluid vortex, as well as the velocity with respect to laminar fluid flow, is reasonable.

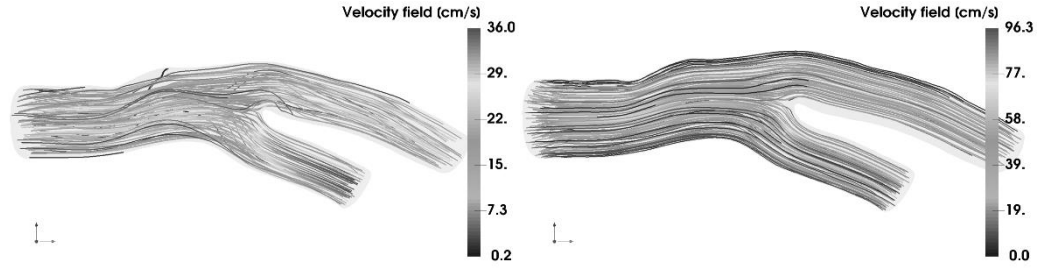

Step 21

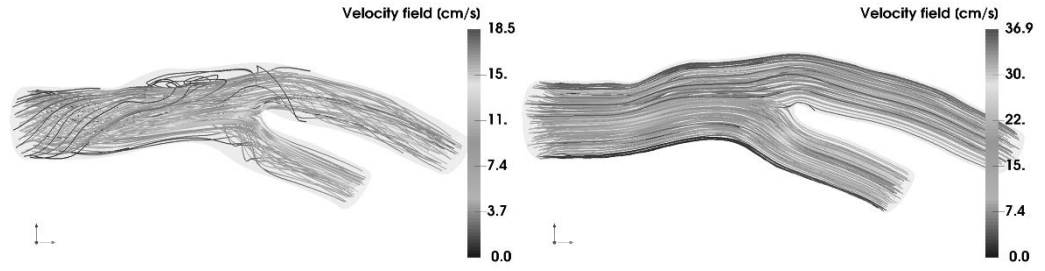

Step 42

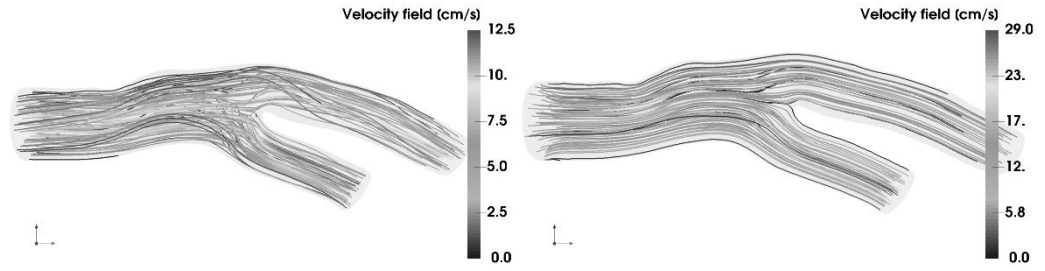

Step 160

a) b)

Fig. 6. Comparison of laminar and turbulent flow case for same Reynolds number 679.

4. Conclusions

In this paper, we have presented turbulent finite element model (a two-equation) because it can be implemented across the viscous sublayer, which can neglect the usage of wall stress function. Regarding the calculation of the basic physical quantities that characterize turbulent flow, we have used and implicit integration of equations. This novel concept and finite element model is also integrated into our multifunction, in-house, software package PAK. Geometry and finite element mesh of the artery is generated by in-house software STL2FEM. Further development will include varying of FE mesh quality which can serve as an improvement regarding velocity field results and quality of other turbulent models using the introduced finite element method. Also, development can go in a direction of using real geometries, obtained from CT scanners, and usage of clinical data which can serve as a basis for creating a certain patient database for a clinical research.

Acknowledgement: The research was funded by Serbian Ministry of Education, Science, and Technological Development, (grants 451-03-09/2021-14/200378 (Institute for Information Technologies, University of Kragujevac) and 451-03-9/2021-14/200107 (Faculty of Engineering, University of Kragujevac)).

References

Arbogast T, Cowsar L, Wheeler M, Yotov I (2000). Mixed Finite Element Methods on Nonmatching Multiblock Grids, SIAM J. Numer. Anal, 37, no. 4, 1295–1315.

Bassi F, Crivellini A, Rebay S, Savini M (2005). Discontinuous Galerkin solution of the Reynolds-averaged Navier–Stokes and k–w turbulence model equations, Computers & Fluids, 34, 507–540.

Bassi F, Ghidoni A, Perbellini A, Rebay S, Crivellini A, Franchina N, Savini M (2014). A high-order Discontinuous Galerkin solver for the incompressible RANS and k–w turbulence model equations, Computers & Fluids, 98, 54–68.

Bathe K. J (2006). Finite Element Procedures, 2nd ed., Klaus-Jurgen Bathe.

Blagojević M, Nikolić A, Živković M, Stanković G, Živković M (2013). Influence of block's topologies on endothelial shear stress observed in cfd analysis of artery bifurcation, Acta of Bioengineering and Biomechanics, 15, no. 1, 97-104.

Blagojevic M, Nikolic A, Zivkovic M, Zivkovic M, Stankovic G (2014). A novel framework for fluid/structure interaction in rapid subject-specific simulations of blood flow in coronary artery bifurcation, Vojnosanit Pregl, 71, no. 3, 285-292.

Boussinesq J (1877). Essai sur la théorie des eaux courantes, Mémoires présentés par divers savants à l'Académie des Sciences.

B. Materialise NV (2017). Mimics software 20.0.

Conti M, Long C, Marconi M, Berchiolli R, Bazilevs Y, Reali A (2016). Carotid artery hemodynamics before and after stenting: A patient specific CFD study, Computers & Fluids, 141, 62-74.

Ferziger J, Peric M (2002). Computational Methods for Fluid Dynamics, 3rd ed ed., NewYork, Springer-Verlag Berlin Heidelberg.

Goubergrits L, Affeld K, Fernandez-Brittoy J, Falcon L (2003). Investigation of geometry and atherosclerosis in the human carotid bifurcations, Journal of Mechanics in Medicine and Biology, 3, no. 1, 31-48.

James A, Berk G, Charles L (2005). ParaView: An End-User Tool for Large Data Visualization, Visualization Handbook, Elsevier, ISBN-13: 978-0123875822.

Jovic S, Driver D. M (1994). Backward-facing step measurements at low reynolds number Reh=5000, NASA Technical Memorandum 108807.

Kojić M, Filipović N, Stojanović B, Kojić N (2008). Computer Modeling in Bioengineering, John Wiley & Sons Ltd, Chichester, UK.

Kojić M, Milosevic M, Simic V, Fleming K. E. J, Nizzero S, Kojic N, Ziemys A, Ferrari M (2017). A composite smeared finite element for mass transport in capillary systems and biological tissue, Computer Methods in Applied Mechanics and Engineering, 324, 413-437.

Kojić M, Slavković R, Živković M, Filipović N, Grujović N, Milosevic M (2020). PAK-finite element program for linear and nonlinear analysis with fluid flow and heat transfer. [Online]. Available: http://www.bioirc.ac.rs/index.php/software/5-pak.

Li Z, Hoagg J. B, Martin A, Bailey S (2018). Retrospective cost adaptive Reynolds-averaged Navier–Stokes k–w model for data-driven unsteady turbulent simulations, Journal of Computational Physics, 357, 353-374.

McDonough J. M (2007). Introductory Lectures on Turbulence, Physics, Mathematics and Modeling, Departments of Mechanical Engineering and Mathematics, University of Kentucky.

Milosevic M, Simic V, Milicevic B, Koay E, Ferrari M, Ziemys A, Kojic M (2018). Correction function for accuracy improvement of the Composite Smeared Finite Element for diffusive transport in biological tissue systems, Computer Methods in Applied Mechanics and Engineering, 338, 97-116.

Nikolić A, Topalović M, Simić V, Filipović N (2021). Turbulent finite element model applied for blood flow calculation in arterial bifurcation, Computer methods and programs in biomedicine, 209, no. 9, In press.

Owida A, Do H, Morsi Y (2012). Numerical analysis of coronary artery bypass grafts: An overview, Computer Methods and Programs in Biomedicine, 108, no. 2, 689–705.

Shi Y, Lawford P, Hose R (2011). Review of Zero-D and 1-D Models of Blood Flow in the Cardiovascular System, Biomed. Eng., vol. 10, no. 33.

Soulis J, Lampri O, Fytanidis D, Giannoglou G (2011). Relative Residence Time and Oscillatory Shear Index of Non-Newtonian Flow Models in Aorta, in Biomedical Engineering, 10th International Workshop on, Kos, Greece.

Tomboulides A, Aithal S, Fischer P, Merzari E, Obabko A, Shaver D (2018). A novel numerical treatment of the near-wall regions in the k-w class of RANS models, International Journal of Heat and Fluid Flow, 72, 186-199.

Weydahl E, Moore J (2001). Dynamic curvature strongly affects wall shear rates in a coronary artery bifurcation model, Journal of Biomechanics, 34, no. 9, 1189–1196.

Wilcox D. C (1988). Reassessment of the scale-determining equation for advanced turbulence models, AIAA Journal, 26, no. 11, 1299-1310.

Wilcox D. C (1994). Turbulence Modeling for CFD, DCW Industries, Inc.

Wilcox D. C (2006). Turbulence Modeling for CFD, 3rd edition, La Canada, CA: DCW Industries, Inc.